Novel action of BAPTA series chelators on intrinsic K^+ currents in rat hippocampal neurones

B. Lancaster and A. M. Batchelor

Wolfson Institute for Biomedical Research, University College London, Gower Street, London WC1E 6BT, UK

1. Whole-cell recordings were made from rat CA1 neurones in brain slices. When electrodes contained diazo-2 (2 mM) or dibromo BAPTA (1 mM) a large steady-state outward current (hundreds of picoamps) developed within 5 min of breakthrough at a V_H of -60 mV. BAPTA itself (1 mM) caused qualitatively similar but smaller effects.

2. The outward current was accompanied by increased conductance with a null potential close to the calculated K^+ equilibrium potential (E_K) of -110 mV. Development of outward current occurred concurrently with progressive loss of slow AHP tail current (I_{sAHP}) evoked by brief depolarizations. The peak latency of I_{sAHP} increased during the onset of chelator action.

3. The persistent outward current was reversibly inhibited by noradrenaline (10 μM) or isoprenaline (2–5 μM), and completely prevented by 8-bromoadenosine 3′,5′ cyclic mono-phosphate (8-Br cAMP; 100 μM) or QX-314 (10 mM) in recording electrodes. After development of outward current, diazo-2 photolysis caused inward current and decreased conductance. Both flash- and noradrenergic-sensitive responses were inwardly rectifying outward currents with null potentials close to E_K.

4. The outward current induced by dibromo BAPTA was not blocked by internal EGTA (10 mM). However, experiments incorporating Ca^{2+} influx or Ca^{2+} loading of the buffer indicate that Ca^{2+} facilitated the outward current.

5. The outward currents induced by dibromo BAPTA or diazo-2 were not associated with significant changes in resting $[Ca^{2+}]_i$. Regions of the cell contributing to the outward current were deduced from measurements of fura-2 diffusion. These were compared with regions of $[Ca^{2+}]_i$ elevation during I_{sAHP}.

6. These results are consistent with the hypothesis that the BAPTA series Ca^{2+} buffers can activate those Ca^{2+}-activated K^+ channels that underlie the slow AHP, without the predicted elevation of bulk $[Ca^{2+}]_i$. Therefore these results cannot be interpreted solely in terms of Ca^{2+} concentration changes, although the observations illustrate a novel, investigative role for these compounds in the study of Ca^{2+}-dependent processes.

The Ca^{2+} buffer BAPTA and its derivatives are used widely for measurement and manipulation of intracellular free Ca^{2+} concentration ($[Ca^{2+}]_i$). Studies with these compounds have occasionally included the parenthetic observation of hyper-polarization or outward current in association with their use (Schwindt *et al.* 1992*b*; Zhang *et al.* 1995; Velumian & Carlen, 1999). Since Ca^{2+} buffers may load with Ca^{2+} after introduction into cells (Mulkey & Zucker, 1993) or from impurities in salts, a persistent Ca^{2+}-dependent K^+ current has been suggested as the basis for this tonic outward current (Zhang *et al.* 1995; Velumian & Carlen, 1999), analogous to the likely explanation for the hyperpolarized

membrane potential observed with Ca^{2+}-loaded nitr-5 (Lancaster & Zucker, 1994).

This paper reports a quantitative investigation of this outward current using, principally, two BAPTA-derived Ca^{2+} buffers, diazo-2 and dibromo BAPTA. Diazo-2 is photolabile (unphotolysed K_D 2·2 μM, photolysed K_D 73 nM; Adams *et al.* 1989), thus allowing a convenient change of buffer properties during the experiment. Dibromo BAPTA has a K_D (1·5 μM, Pethig *et al.* 1989) in the same range as unphotolysed diazo-2, but since it is not photolabile, we could use this compound in conjunction with ratiometric Ca^{2+} imaging with fura-2. We conclude that the outward

current is generated by tonic activation of I_{sAHP} that occurs without detectable bulk $[Ca^{2+}]_i$ elevation.

The I_{sAHP}, which is presumed to be generated by SK-type Ca^{2+}-activated K^+ channels, is conventionally studied with the Ca^{2+} influx accompanying action potentials or voltage clamp depolarizations. The physiological relevance of this approach is offset by the natural spatial and temporal variability of the Ca^{2+} signal or Ca^{2+}-dependent process. Spatial variability will result from uneven distribution of calcium channels or their targets, in addition to the uncertainties of action potential propagation/depolarization over the soma–dendritic axis. Temporal variability is an intrinsic feature of depolarization-evoked Ca^{2+} entry which is initially localized to domains of high concentration on a millisecond time scale before dissipating to a reduced but less localized Ca^{2+} signal lasting seconds (Llinás et al. 1992; Monck et al. 1994; Eilers et al. 1995). The resultant ambiguities have allowed different interpretations of Ca^{2+} dependence of the Ca^{2+}-activated K^+ current which produces slow afterhyperpolarizations (sAHPs) in CA1 pyramidal cells. The time course of this current and some pharmacological properties have been variously attributed to direct activation by buffered Ca^{2+} (Lancaster & Zucker, 1994; Zhang et al. 1995), Ca^{2+}-induced Ca^{2+} release (Sah & McLachlan, 1991; Tanabe et al. 1998), Ca^{2+} in conjunction with other second messengers (Schwindt et al. 1992a; Lasser-Ross et al. 1997) and delayed facilitation (reopening) of calcium channels following depolarization (Marrion & Tavalin, 1998).

These experiments with BAPTA-derived buffers allowed investigation of Ca^{2+}-activated K^+ current without depolarization-induced Ca^{2+} influx and thereby clarification of some issues which have been difficult to address by other methods. This principle has been used previously (Lancaster & Zucker, 1994; Sah & Clements, 1999) in experiments using flash photolytic release of Ca^{2+}, but these are still transient events generated from a gradually depleting source as the buffer is photolysed. A steady-state Ca^{2+}-activated K^+ current is a major technical improvement which is much more amenable to investigation. In addition, imaging of the isosbestic (Ca^{2+}-insensitive) wavelength of fura-2 allowed us to track the progress of dye after breakthrough while monitoring the electrical properties of the cell. With this novel information we can place some constraints on the spatial localization of membrane currents generated by the calcium chelators.

Some of this material has been published in abstract form (Lancaster & Batchelor, 1999).

METHODS

Tissue preparation

Hippocampi were obtained from 14- to 21-day-old rat pups after cervical dislocation and decapitation. Transverse slices (400 μm) were cut using a Vibratome (TPI-1000, Intracel, Royston, UK) and maintained at room temperature (15–30 °C) at the interface between a moist oxygenated atmosphere and a medium of the following composition (mM): NaCl, 119; KCl, 2·5; MgCl$_2$, 1·3; CaCl$_2$, 2·0; NaH$_2$PO$_4$, 1·0; NaHCO$_3$, 26; glucose, 11. This solution bubbled with 95% O$_2$–5% CO$_2$ was also perfused in the recording chamber where slices were submerged and temperature maintained between 28–30 °C. Drugs were obtained from BDH (Poole, Dorset, UK) unless specified otherwise. Other chemicals used in the external solution were isoprenaline bitartrate and (−)-noradrenaline bitartrate (Sigma, St Louis, MO, USA).

Electrophysiology

Recording pipettes were fabricated with a horizontal puller (Sutter Instruments, Novato, CA, USA) using thin-walled glass containing a filament (Clark Electromedical, Pangbourne, UK). They were filled with the following solution (mM): potassium methylsulphate, 150 (Phase Separations, Wales); KCl, 10; Hepes, 10 (Sigma); NaCl, 4; MgATP, 4 (Sigma); NaGTP, 0·4 (Sigma). Osmolarity was adjusted to 280–290 mosmol l^{-1} and pH to 7·35–7·4 with KOH. Final K^+ concentration was 160 mM. The methylsulphate anion was used because it has been shown to preserve I_{sAHP} in a form similar to that observed with sharp electrode recordings (Lancaster & Adams, 1986; Zhang et al. 1994). Stock solutions of diazo-2 or dibromo BAPTA (Molecular Probes Europe, The Netherlands) were made in 150 mM KMops (pH 7·4, Sigma) and stored as aliquots at −20 °C before dilution in the pipette solution. Pipette solution occasionally included 2 mM BAPTA, 10 mM EGTA (Sigma, pH 7·3–7·4 with KOH), QX-314 (10 mM, Alomone Labs, Jerusalem, Israel) or 8-Br cAMP (100 μM, Sigma). Open pipette resistance was 2–4 MΩ. Whole-cell patch voltage clamp recordings were obtained from neurones in the CA1 stratum pyramidale without visual identification. Access resistances ranged from 8 to 25 MΩ. Series resistance compensation was set to 70–80% with a 10 μs lag. Membrane currents were recorded and filtered (500 Hz) using an Axopatch 1D (Axon Instruments, Foster City, CA, USA) and digitized at 1 kHz using a Digidata 1200 and pCLAMP 6 software (Axon Instruments) on an Intel 486-based personal computer. Analysis was performed using pCLAMP 6 and Origin (MicroCal Software Inc., Northampton, MA, USA).

Photolysis of diazo-2 was accomplished using a xenon arc flashlamp (Rapp design, Hi-Tech Scientific, Salisbury, UK) focussed on the recording chamber to illuminate a spot covering the CA1 region. Repeatability of flash actions indicates that photolysis is typically incomplete following a single flash (see also Lancaster & Zucker, 1994). This is caused by UV scattering and absorbance according to tissue and solution depth. Additionally, the absorption spectrum of diazo-2 (Adams et al. 1989) has a bandwidth that comprises less than 20% of the total energy output of the 1 ms flash discharge.

Calcium imaging

To estimate the free cytoplasmic calcium ion concentration, $[Ca^{2+}]_i$, we added the calcium indicator dye fura-2 (200 μM of the penta-potassium salt; Molecular Probes) to the relevant pipette solutions. The emitted fluorescence of fura-2 was recorded using a cooled CCD camera (C4880-81 in 10-bit mode, 2 × 2 binning, Hamamatsu Photonics, Hamamatsu City, Japan) mounted on an upright microscope (Axioskop-FS, Zeiss, Welwyn Garden City, UK). The cells were imaged using a × 40 water immersion lens (Achroplan, numerical aperture 0·75, Zeiss). Excitation light was switched between 340 nm (half-width 14 nm, Chroma Technology, Brattleboro, VT, USA), 360 nm (half-width 10 nm, Omega Optical, Brattleboro, VT, USA) and 380 nm (half-width 14 nm, Chroma Technology) by a filter wheel (Lambda 10-2, Sutter Instruments) under the control of the image acquisition software (Acquisition Manager 3.10, Kinetic Imaging, Liverpool, UK). Image triplets (exposure 223 ms, separation ~680 ms) were acquired every 7 s.

$[Ca^{2+}]_i$ was estimated using standard methods (Grynkiewicz *et al.* 1985) using a ratio of the fluorescence excited at 340 and 380 nm, where $[Ca^{2+}]_i = K_D(S_{f2}/S_{b2})(R - R_{min}/R_{max} - R)$, where R_{min} and R_{max} are the fluorescence ratios in the absence and presence of saturating Ca^{2+}, and S_{f2} and S_{b2} are 380 nm fluorescence in zero and saturating calcium, respectively. Values for R_{max} (6·70), R_{min} (0·43) and S_{f2}/S_{b2} (5·95) were obtained by recording the fluorescence of the somatic region with either saturating (internal solution plus 10 mM $CaCl_2$) or zero calcium levels (i.e. +10 mM EGTA). The K_D of fura-2 under our conditions was estimated to be ~200 nM.

Faster temporal resolution (15–20 Hz) during I_{sAHP} was achieved with single wavelength imaging of fura-2 at 380 nm. The fluorescence signal is presented as $-\Delta F/F$ (per cent), where F is the mean value 1 s prior to depolarization. Single wavelength measurements were bracketed by ratio measurements; this allowed conversion of the fluorescence changes to approximate $[Ca^{2+}]_i$.

Calcium imaging during diazo-2 photolysis experiments was performed using the visible wavelength Ca^{2+} indicator calcium green-1 (200 μM, tetrapotassium salt, Molecular Probes). This was necessary to avoid photolysis of the diazo-2 by the UV wavelengths used to excite fura-2. Diazo-2 photolysis was performed using the

xenon microscope lamp filtered through a UG11 filter (330 nm peak, H. V. Skan Ltd, Solihull, UK) installed in the filter wheel.

Data were analysed using Lucida 3.53 (Kinetic Imaging), Origin 4.1 (Microcal) and Excel-97 (Microsoft Inc.). Statistical significance was assessed using Student's unpaired t test.

The 'blind' patch-recording technique we employed necessitates the use of positive pressure for successful seal formation. This results in significant levels of fluorescence due to extracellular dye. The problem is particularly relevant in the experiments where we monitor the fluorescence immediately following breakthrough, i.e. during the development of the outward current. This background signal is neither stationary during the experiment (due to washing away the dye) nor is it evenly distributed throughout the field of view. Therefore a single background area will not provide adequate background correction for all parts of the image acquired. Instead, correction was made using matched background areas adjacent to the cellular region of interest for each time point. Electrophysiology was as before but using an Axopatch 200B for voltage clamp experiments or an Axoclamp-2A for acquisition of current clamp data. Some imaging data, not involving I_{sAHP}, were acquired at room temperature with no obvious effect on resting $[Ca^{2+}]_i$.
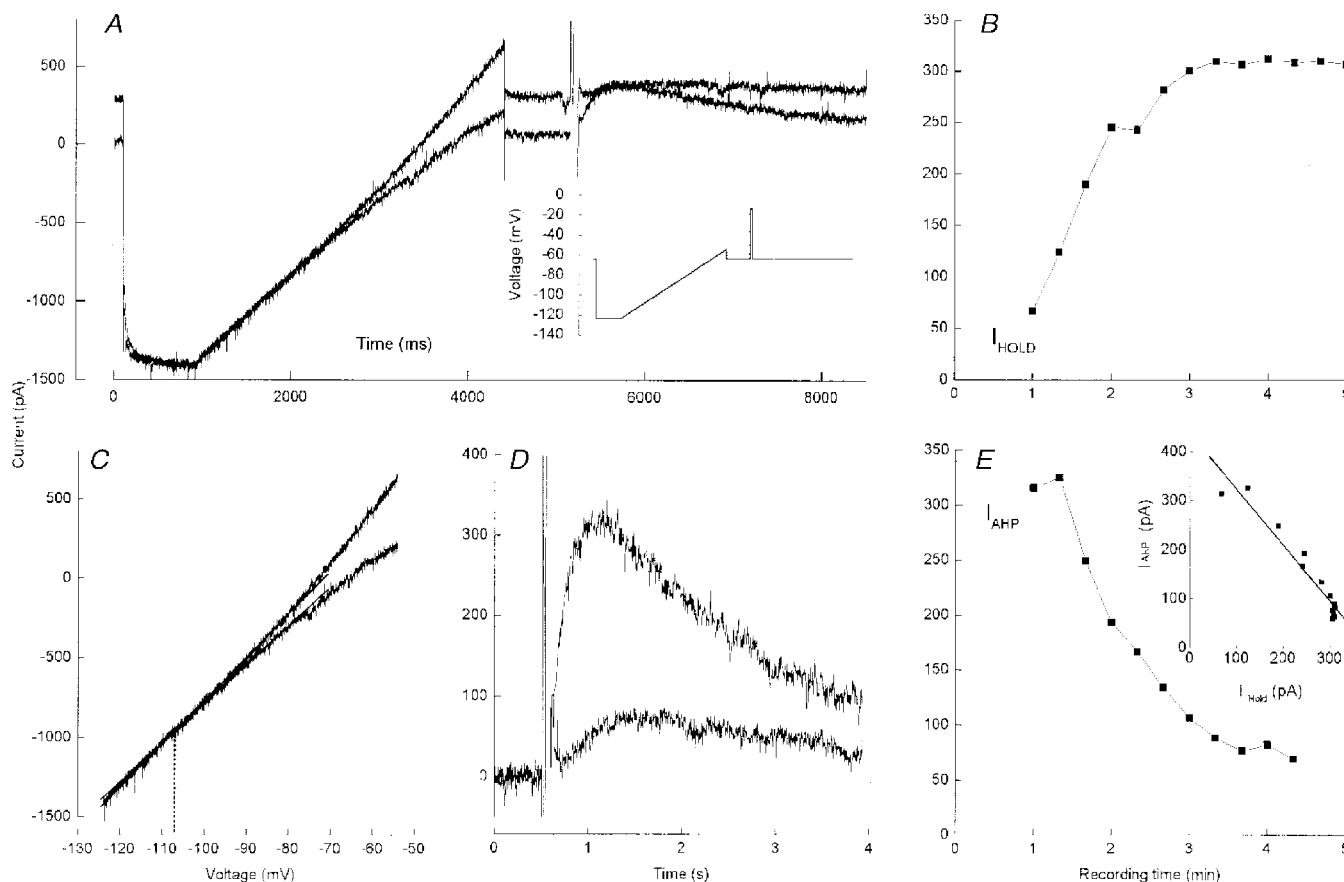

Figure 1. Characteristics of outward current produced by intracellular diazo-2

A, membrane current in response to the voltage protocol shown in the inset, before and after development of a steady-state outward current. *B*, time course of outward current development; the abscissa represents time of whole-cell recording. *C*, current–voltage relation of the slope regions from *A*. The data were fitted with a straight line between −80 and −90 mV. Extrapolation of these fits crosses at −107 mV. *D*, loss of the depolarization-evoked I_{sAHP} is accompanied by an increase in the time to peak of this current. *E*, time course of the loss of I_{sAHP} is closely correlated (inset, $R = -0.97$) with the development of the outward current.

RESULTS

Diffusion of diazo-2 or dibromo BAPTA into the cell was associated with an outward current which peaked within 4–5 min of seal breakthrough to whole-cell recording. This was routinely observed in the presence of the BAPTA-derived chelators ($n = 87/88$ cells), the single exception being a putative interneurone characterized by a brief spike duration (400 μs at half-amplitude) and the ability to fire at high frequency (up to 260 Hz). Figure 1A shows sample current traces from the voltage protocol (inset) designed to assess electrophysiological changes associated with the outward current. A voltage step from hold (V_H, −60 mV) to −120 mV prior to a 3 s ramp to −50 mV produced a quasi-steady-state current–voltage (I–V) relation. This was followed by an 80 ms step to −10 mV to evoke unclamped Ca^{2+} influx which initially was able to generate I_{sAHP} (lower trace in Fig. 1A). The second superimposed trace in Fig. 1A (2 mM diazo-2 in the pipette) was obtained after a 300 pA outward current had developed with a time course shown in

Fig. 1B. The extra current was associated with an increase in conductance, as indicated by the increased current step at the end of the ramp and by the increased slope of the I–V plot in Fig. 1C. The I–V plots were fitted with a straight line between −80 and −90 mV. The extrapolation of this fit is visible in Fig. 1C and the intersection occurs at −107 mV, which is close to the calculated E_K of −110 mV for these experiments. Another characteristic of the action of diazo-2 was loss of the depolarization-evoked I_{sAHP} in tandem with the development of outward current (Fig. 1A, D and E). These two events are strongly correlated (Fig. 1E inset) and the I_{sAHP} peak shows a shift to longer latency during this process (Fig. 1D). In some cells the buffer produced an additional inward current that was apparent during steps to −100 mV. In this paper we confine ourselves to study of the K^+ conductance increase.

Diazo-2 is a photosensitive Ca^{2+} buffer which undergoes an increase in affinity upon photolysis (unphotolysed K_D 2·2 μm, photolysed K_D 73 nM). Photolysis should therefore
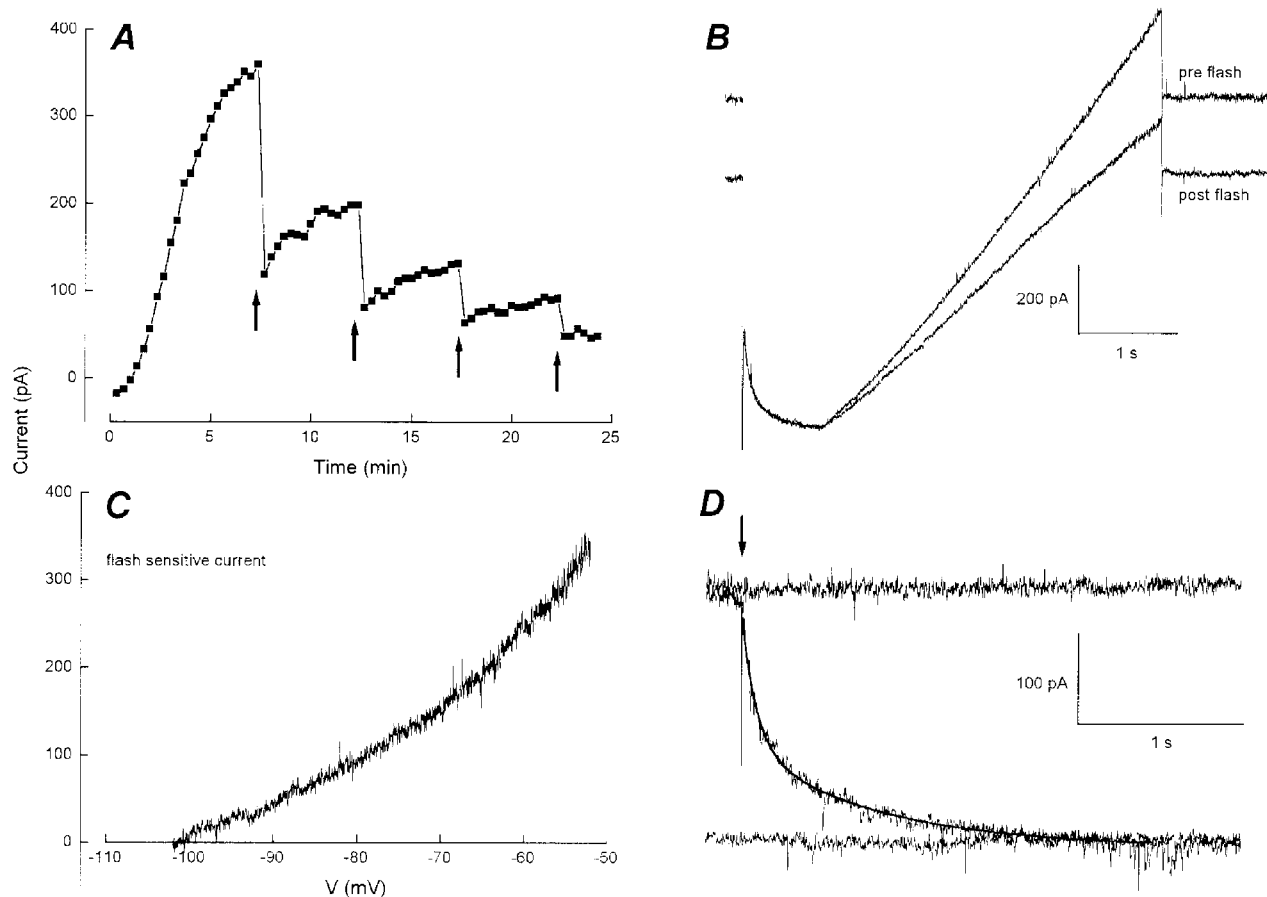

Figure 2. Effects of diazo-2 photolysis on persistent outward current

A, UV flashes (150 J, arrows) cause partial reversal of outward current; the flashes are followed by incomplete recovery leading to a cumulative loss of outward current after 4 flashes. B, pre- and post-flash membrane current traces (V_H −60 mV, step to −100 mV for 500 ms, then a 3 s ramp to −50 mV). The post-flash inward current is associated with a reduction in slope and chord conductance. C, flash-sensitive current obtained by subtraction of slope regions in B. D, data from a different cell illustrating the time course of outward current decay following a 150 J flash (arrow). The smooth curve is a bi-exponential fit with $\tau_1 = 89$ ms and $\tau_2 = 799$ ms.

reduce the availability of Ca^{2+} within the cell and thereby test the hypothesis that the outward current is due to persistent Ca^{2+}-activated K^+ current, as previously suggested (Zhang *et al.* 1995; Velumian & Carlen, 1999). An example of this experiment is illustrated in Fig. 2*A* where 150 J flash discharges progressively reversed the outward current. The partial reversibility or recovery from the flash was a common feature of this manipulation (20/22 cells). Individual traces immediately before and after the first flash are shown in Fig. 2*B*; the inward shift in holding current caused by the flash was accompanied by a decrease in membrane conductance. The slope regions in Fig. 2*B* were subtracted to produce the *I–V* relation of flash-sensitive current in Fig. 2*C*. The current had a null potential between −100 and −110 mV and showed inward rectification as expected for K^+ current under asymmetric conditions. The time course of outward current relaxation following photolysis is illustrated in Fig. 2*D*. Records at 20 s intervals show current traces before, during and after a flash (arrow). The discharge, accompanied by a brief spike artifact, was

followed by a current relaxation which required two time constants for an adequate fit to the data. This analysis was performed in six cells yielding $\tau_1 = 88 \pm 17$ ms and $\tau_2 = 962 \pm 239$ ms (means ± s.e.m.).

The flash sensitivity shown in Fig. 2 would normally be taken as evidence for a Ca^{2+} dependence of the tonically activated outward K^+ current (but see Figs 7 and 8). CA1 pyramidal cells contain at least three Ca^{2+}-activated K^+ currents. The BK type, which is TEA sensitive, is unlikely to be involved since implausibly high $[Ca^{2+}]_i$ (Barrett *et al.* 1982; Yoshida *et al.* 1991) would be required to maintain activity at potentials negative to rest as in Figs 1 and 2. The most likely candidates are therefore apamin-sensitive and -insensitive SK-type Ca^{2+}-activated K^+ currents (Stocker *et al.* 1999). Our attention focussed on the I_{sAHP} which is lost during outward current development; this is an apamin-insensitive current. There are no selective toxins for this current but it has a well described sensitivity to β-noradrenergic receptor agonists (Madison & Nicoll, 1986). We therefore used noradrenaline or isoprenaline as a
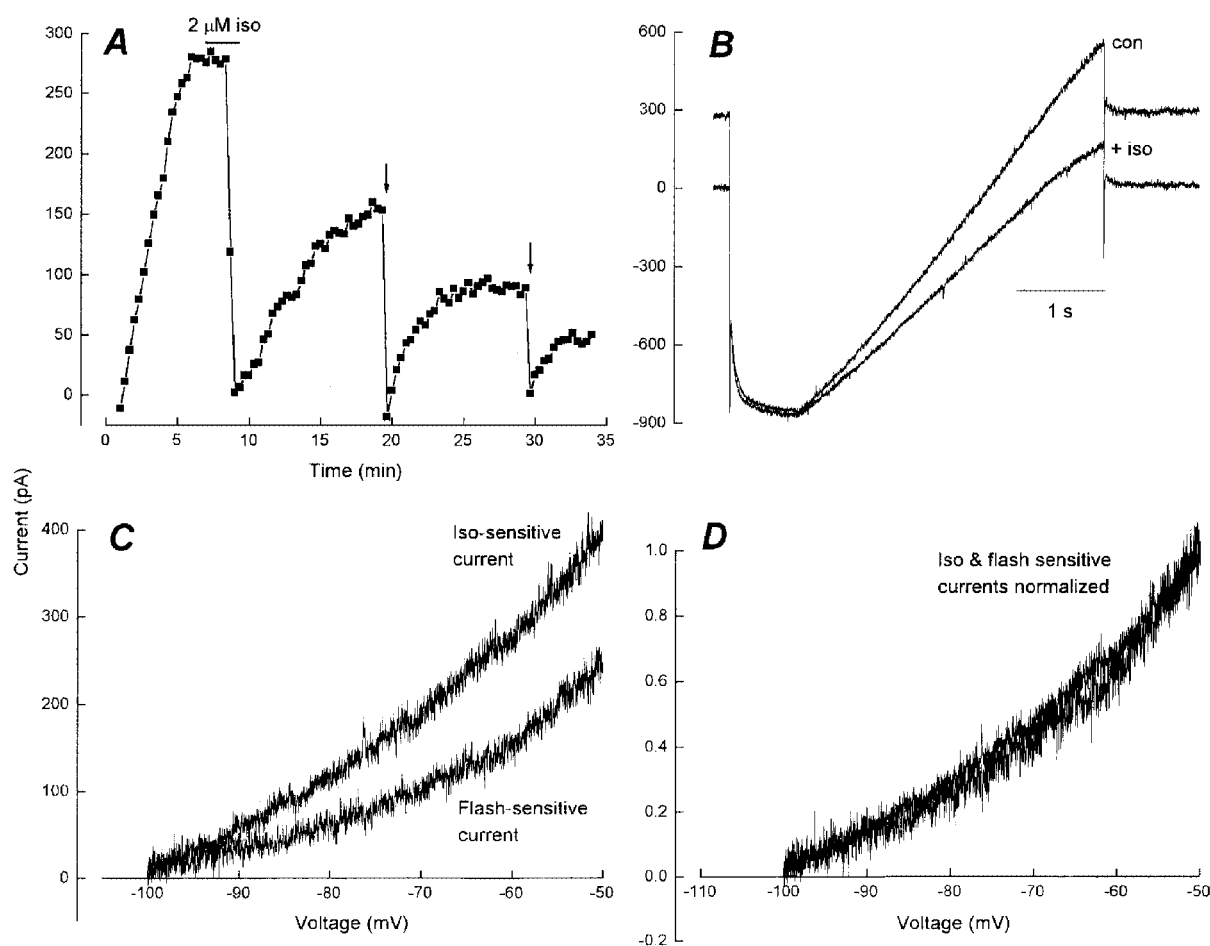

Figure 3. Correspondence of UV and noradrenergic sensitivity of outward current

A, action of 2 μM isoprenaline (iso) and UV flashes (150 J, arrows) on the outward current caused by diazo-2. *B*, current traces (V_H −60 mV, step to −100 mV then a 3 s ramp to −50 mV) before (con) and after isoprenaline (+iso) treatment show an inward current accompanied by a decrease in membrane conductance. *C*, isoprenaline- and flash-sensitive currents obtained by subtraction. *D*, normalization of the currents in *C*.

pharmacological test on the outward current caused by diazo-2. Figure 3*A* shows that the diazo-2-dependent outward current was completely and reversibly sensitive to the β-specific agonist isoprenaline (2 μM) or UV flashes. Sample traces for control and isoprenaline application are shown in Fig. 3*B*. Subtracted slope regions under the relevant conditions generated currents that were isoprenaline and flash sensitive (Fig. 3*C*). After normalization to peak amplitude, these currents displayed identical *I–V* characteristics (Fig. 3*D*) of an inwardly rectifying outward current with a null potential close to E_K.

Summary data for the membrane actions of diazo-2 are shown graphically in Fig. 4. In comparison with control recordings without any exogenous Ca^{2+} buffer, 2 mM diazo-2 was associated with a clear development of outward current with an amplitude of 246 ± 28 pA (mean $\pm$ s.e.m., $n = 20$, holding potential -60 mV) 5 min after breakthrough (Fig. 4*A*). At this time, control values were -34 ± 22 pA ($n = 10$). Recordings from cells which showed inward current drift (and would normally be jettisoned) were not excluded from control data since it was not possible to make any comparable selection for the other data sets. From subsets of the diazo-2 cells, summary data for the effects of photolysis (first flash discharge) and noradrenergic action on holding current are shown in Fig. 4*B* and *C*, respectively.

The *x*-axes have been normalized to the time of manipulation ($t = 0$). The mean reduction in current following a flash was 80% (assuming a starting point at zero current, $n = 9$). The equivalent reduction caused by noradrenergic action was 94% ($n = 7$).

To test whether the outward current was a unique property of the photolabile compound, we performed a range of similar experiments with the related Ca^{2+} buffer dibromo BAPTA. This compound has a similar K_D ($1{\cdot}5\ \mu$M) to unphotolysed diazo-2 without being UV sensitive, thus permitting further experiments in conjunction with fura-2 to determine the $[Ca^{2+}]_i$ that was associated with the putative Ca^{2+}-dependent outward current. Sample data from two cells recorded with 1 mM dibromo BAPTA in the pipette are shown in Fig. 5. The traces in Fig. 5*A* are the first and final sweeps from the time course of outward current development plotted in Fig. 5*B*. The outward current generated by dibromo BAPTA was accompanied by an increase in conductance over the range -100 to -50 mV and a concurrent loss of I_{sAHP} during which the prolongation of peak latency was again observed (Fig. 5*A* inset shows sweeps 1 and 6). The *I–V* characteristics of the subtracted record of Fig. 5*C* reveal an inwardly rectifying outward current with a null potential at -104 mV. The data in Fig. 5*D* are from a different cell which illustrates reversible

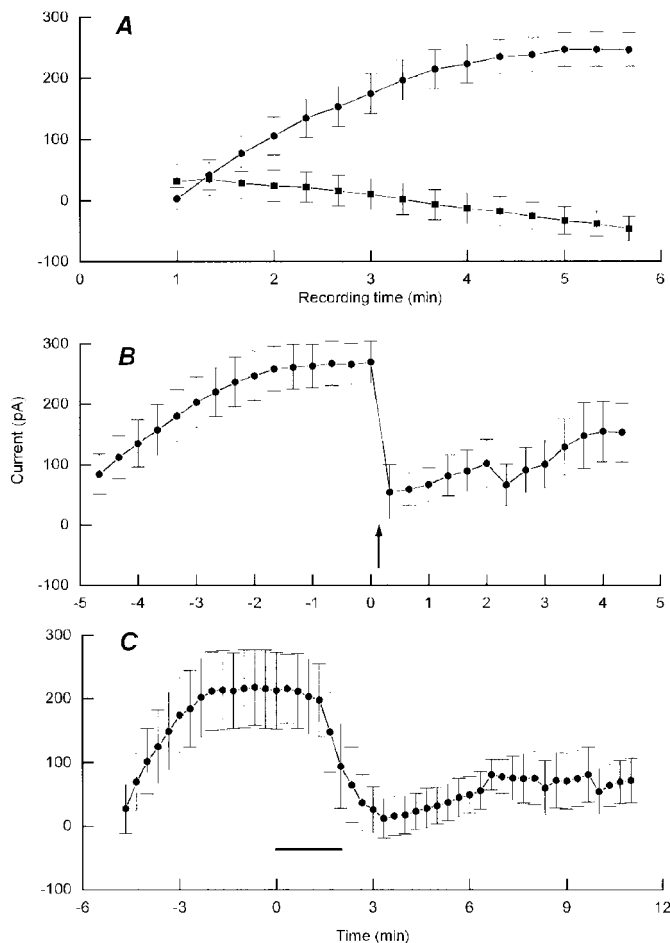**Figure 4. Summary of membrane properties with diazo-2**

A, plot of holding current (V_H -60 mV) against time of whole-cell recording for control (no calcium buffer, ■, $n = 10$) and diazo-2 (2 mM, ●, $n = 20$) recordings. Points in this figure represent means $\pm$ s.e.m. of absolute current measurements. *B*, effect of a 150 J UV flash (arrow) on outward current (mean current $\pm$ s.e.m. is reduced from 269 ± 35 to 55 ± 45 pA, $n = 9$). *C*, effect of a 2 min application (bar) of either 2 μM isoprenaline or 10 μM noradrenaline (mean current $\pm$ s.e.m. is reduced from 218 ± 60 to 12 ± 31 pA, $n = 7$). The abscissa for *B* and *C* is normalized to the time of manipulation and does not represent absolute recording time.

inhibition of the outward current by noradrenaline. The inset shows pseudo-steady-state *I–V* plots before and after current development, and following noradrenaline action. The zero current values from this plot indicate that under current clamp conditions the outward current would hyperpolarize the cell by 9 mV. These changes in membrane properties were reliably observed using dibromo BAPTA and appeared qualitatively similar to the action of diazo-2. The summary data in Fig. 6 give the time course of outward current development which reached a value of 548 ± 91 pA ($n = 10$, holding potential −60 mV) 5 min after breakthrough (Fig. 6, ●). To assess any contribution of depolarization-evoked Ca^{2+} influx to development of this outward current, a series of experiments were performed in which resting conductance was monitored only with hyperpolarizing steps (inset in Fig. 6). Under these conditions an outward current still developed and its amplitude

(413 ± 99 pA) 5 min after breakthrough was not significantly different from the data including depolarizing steps (Fig. 6, ○, $P = 0.36$). An average of 50% of the dibromo BAPTA outward current was inhibited by noradrenergic action. As a further test of the correspondence between I_{sAHP} and the outward current we performed a second pharmacological test based on the proposed transduction mechanism for β-adrenergic inhibition of the AHP which includes cAMP and protein kinase A activity (Madison & Nicoll, 1986; Pedarzani & Storm, 1993). Diffusion of 100 μM 8-Br cAMP together with dibromo BAPTA from the pipette (▼, Fig. 6) resulted in a holding current, at 5 min recording time, which was not significantly different ($P = 0.22$) from control pipette solution (8-Br cAMP, −90 ± 43 pA, $n = 7$; control from Fig. 4*A*, −34 ± 22 pA, $n = 10$). This result excludes a major contribution from apamin-sensitive channels to the outward current.
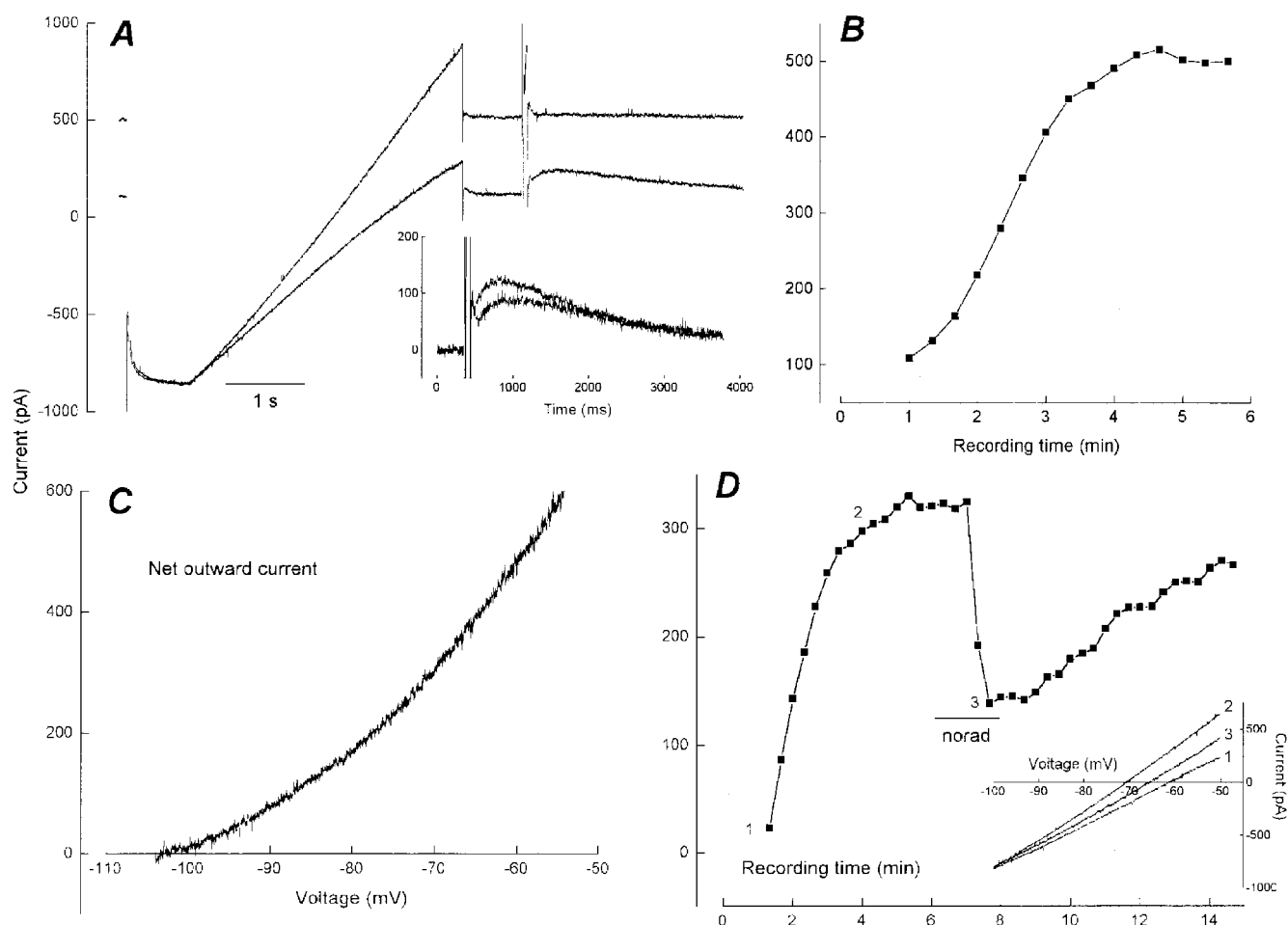

Figure 5. Characteristics of outward current produced by intracellular dibromo BAPTA

A, current traces before and after development of outward current with 1 mM dibromo BAPTA (voltage protocol as in Fig. 1*A*). The outward current is accompanied by increased membrane conductance and progressive loss of I_{sAHP}. The peak latency of I_{sAHP} increases during this process (inset). *B*, time course of outward current development following seal breakthrough at $t = 0$. *C*, *I–V* relation of the dibromo BAPTA-induced outward current obtained by subtraction of the traces in *A*. *D*, data from a different cell illustrating the effect of noradrenaline application (norad, 10 μM, 2 min) on dibromo BAPTA-induced current. Inset shows unsubtracted current slopes for the various conditions; 1, control; 2, outward current; 3, plus noradrenaline.
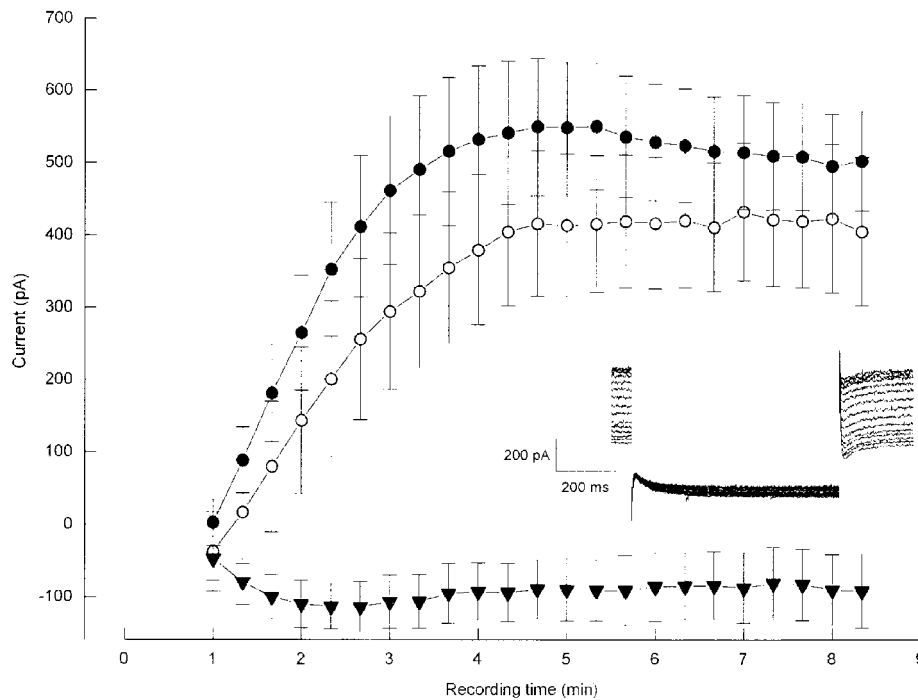
Figure 6. Hydrolysis-resistant cAMP blocks outward current development

Summary data for outward currents evoked by dibromo BAPTA with voltage commands including depolarization (as in Fig. 1A, ●, $n = 10$) or without depolarization (○, $n = 9$). The inset shows traces during outward current development without membrane depolarization (V_H −70 mV, step to −85 mV). ▼, summary data for holding current when recording pipettes contained 1 mM dibromo BAPTA and 100 μM 8-Br cAMP ($n = 7$). All points represent mean ± s.e.m.
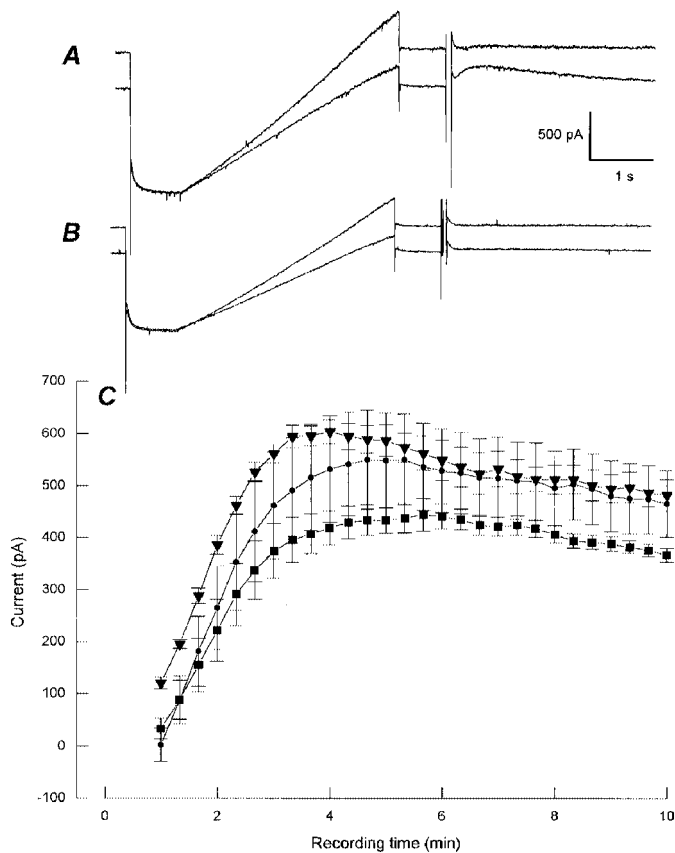

Figure 7. Outward current under high and low Ca²⁺-loading conditions

A, current traces showing effects of 0·5 mM Ca^{2+}−1 mM dibromo BAPTA (voltage protocol as in Fig. 1A). B, current traces showing effects of 10 mM EGTA−1 mM dibromo BAPTA. C, summary data for outward current development with Ca^{2+}-loaded chelator (▼, $n = 5$) or in the presence of EGTA (■, $n = 5$). For comparison, the control data without manipulation of Ca^{2+} (●) are reproduced from Fig. 6. All points represent mean ± s.e.m.

Thus far the data are consistent with persistently active I_{sAHP} underlying the actions of the Ca^{2+} chelators. Opening of SK channels, which are postulated to underlie I_{sAHP}, only requires elevated $[Ca^{2+}]_i$ (Köhler *et al.* 1996; Xia *et al.* 1998), but since depolarization-evoked Ca^{2+} entry was not a prerequisite for the outward current, we performed more explicit tests of Ca^{2+} dependence using high- and low-Ca^{2+} pipette solution. These manipulations also minimise variability resulting from any Ca^{2+} contamination of the pipette solution. For high-Ca^{2+} conditions, 0·5 mM Ca^{2+} was added to produce a 50% loading of the dibromo BAPTA. For low-Ca^{2+} conditions 10 mM EGTA was included with dibromo BAPTA. Outward currents were still observed to develop with high Ca^{2+}, but surprisingly, also with the highly buffered internal solution (Fig. 7*A* and *B*). The ability of EGTA to buffer is shown by the absence of I_{sAHP} following depolarizing steps early in the experiment (Fig. 7*B*). Pooled data for these conditions are presented in Fig. 7*C*. The high-Ca^{2+} and EGTA data are shown in comparison to the previously illustrated dibromo BAPTA curve. The larger errors for these data may reflect the

uncontrolled variable of Ca^{2+} loading in these experiments. The action of unloaded buffer was initially coincident with the EGTA/low-Ca^{2+} data and crossed over to coincide with the Ca^{2+}-loaded curve after 6 min recording time. This observation, plus the slightly faster development of outward current with high-Ca^{2+} internal solution, suggests some involvement of Ca^{2+} in this process, but the clear outward current in the presence of 10 mM EGTA is difficult to reconcile with Ca^{2+} activation of the K^+ current.

To test directly whether any change in bulk $[Ca^{2+}]_i$ is associated with the persistent outward current we measured $[Ca^{2+}]_i$ using the ratiometric dye fura-2, in conjunction with the changes in membrane properties caused by dibromo BAPTA (Fig. 8*A*–*C*). Measurements of $[Ca^{2+}]_i$ were obtained from somatic and dendritic regions as outlined in Fig. 8*A* after careful correction for background signals (see Methods). Different regions of the cell exhibited similar resting $[Ca^{2+}]_i$. These measurements and the outward current recorded from this cell are shown in Fig. 8*B*. The outward current behaved as described previously, reaching a peak of about 420 pA within 4–5 min recording time. The $[Ca^{2+}]_i$
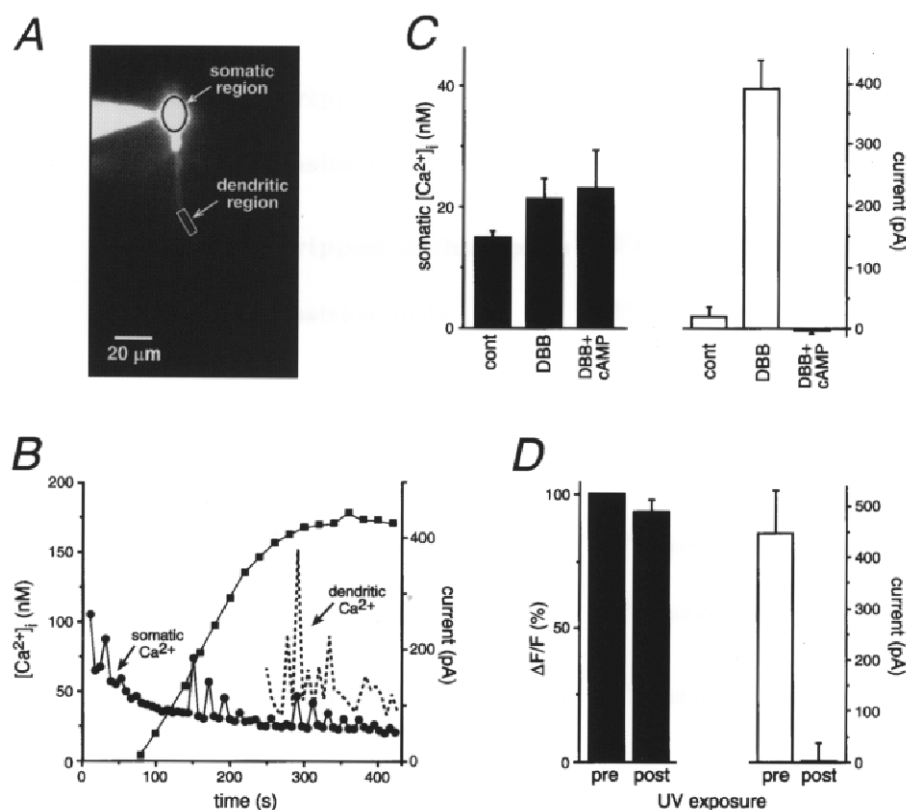

Figure 8. $[Ca^{2+}]_i$ measurements during action of BAPTA series chelators

A, image of a fura-2-filled CA1 cell indicating regions of interest for Ca^{2+} measurements. *B*, data taken from the cell in *A* show $[Ca^{2+}]_i$ in the somatic (●) and dendritic region (dotted line) in conjunction with the development of outward current (■; 1 mM dibromo BAPTA) following breakthrough at $t = 0$ s. Periodic $[Ca^{2+}]_i$ elevations arise from the depolarizing voltage commands. *C*, left panel, mean somatic $[Ca^{2+}]_i$ after 4–5 min recording for control (cont) cells and dibromo BAPTA with (DBB + cAMP) or without 8-Br cAMP (DBB). The right panel shows contemporaneous values of holding current under these conditions. *D*, a comparison of resting calcium green-1 fluorescence and holding current before (pre) and after (post) diazo-2 photolysis.

measurements indicate a baseline value just after break-through of approximately 75 nM which fell to around 25 nM at 4–5 min. Periodic spikes in the $[Ca^{2+}]_i$ signal are due to rhythmic coincidence of the fluorescence measurements (7 s interval) and the electrophysiology (20 s interval) protocol containing the depolarization, but since shutter opening is not exactly coincident with depolarization, the $[Ca^{2+}]_i$ changes are underestimated. The dotted line shows that depolarization-induced Ca^{2+} transients were detectable in the dendrites after development of the outward current. Pooled data for the somatic $[Ca^{2+}]_i$ levels at 4–5 min recording time are given in Fig. 8C for control cells (no buffer) as well as recordings using dibromo BAPTA (DBB) with or without 8-Br cAMP. The outward current was typically maximal at the time of these measurements. The mean somatic $[Ca^{2+}]_i$ for dibromo BAPTA recordings was 21 ± 3 nM ($n = 9$) compared with 15 ± 3 nM ($n = 6$) for control cells. The value for 8-Br cAMP-treated cells (23 ± 6 nM, $n = 6$) was virtually identical to that for dibromo BAPTA alone. Corresponding values of holding current

during the same time period are presented in Fig. 8C (right panel). The dibromo BAPTA-induced current increase in the group of cells used for the $[Ca^{2+}]_i$ measurements above was 392 ± 47 pA ($n = 9$).

The comparison of outward current and resting $[Ca^{2+}]_i$ was made also for diazo-2. In this case we performed the converse experiment of testing whether resting $[Ca^{2+}]_i$ was altered following outward current deactivation by diazo-2 photolysis (Fig. 8D). Constant UV illumination (5–6 s) caused a change in holding current from 446 ± 87 to 2 ± 34 pA ($n = 4$). The resting fluorescence of calcium green-1 following photolysis was not significantly changed (96 ± 4% of control, $P = 0.27$). The presence of active photolysis product was confirmed by a large reduction in the peak fluorescence following depolarization-evoked Ca^{2+} influx (not shown). This was associated with a marked reduction in the rate of decay of the Ca^{2+} signal as expected for an increase in the concentration of a high affinity buffer (Helmchen *et al.* 1996; Lasser-Ross *et al.* 1997). Taken together the electro-physiological and imaging data illustrated in Figs 7 and 8
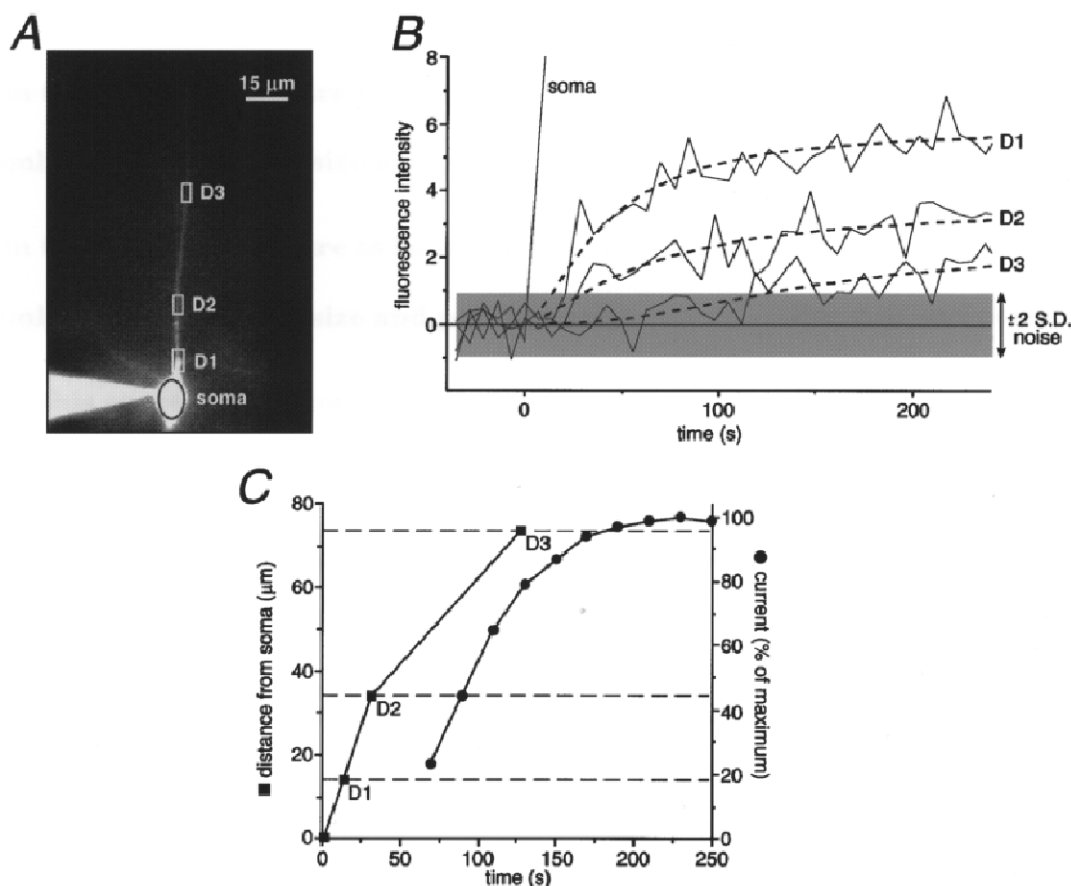

Figure 9. Measurement of dye diffusion constrains location of outward current

A, image of a fura-2-filled CA1 cell indicating regions of interest for fluorescence (360 nm) measurements. *B*, time course of fluorescence intensity (arbitrary units) in the 4 regions of interest following breakthrough ($t = 0$). Dashed lines show sigmoidal fits to the dendritic data. The shaded area represents the noise level. *C*, time taken to reach significant fluorescence values at the dendritic regions delineated in *A* (left axis, ■). The time course of current development is shown by the filled circles (right axis). The *y*-axes intercepts of the dashed lines denote the percentage of the outward current that has developed as the fura-2–dibromo BAPTA reaches the specified dendritic regions.

show that the outward current induced by the chelators has no requirement for elevated $[Ca^{2+}]_i$.

In order to monitor fluorescence from the onset of the recording, the camera was focussed on the pipette tip prior to seal breakthrough. In some cases this focal plane also contained a substantial part of the apical dendrite (Fig. 9A) which gradually filled with the fura-2. In subsequent analysis, placement of regions of interest over the dendrite (D1–D3) allowed us to track the appearance of Ca^{2+}-independent fluorescence (excited at 360 nm) in these regions during the course of the recording. Assuming that fura-2 and dibromo BAPTA have similar mobility within the cell, the progression of the fluorescence signal can be compared with the development of outward current, the principle being that only those parts of the cell which are visible (have dye present) can contribute to the outward current present at that time. This does not prove a contribution from all visible portions of the cell but rather places an outer limit on the possibilities. A semi-quantitative development of this idea is shown in Fig. 9. Fluorescence intensity was measured at the soma and three increasingly distal portions of the apical dendrite (D1–D3) shown in Fig. 9A. Fluorescence intensity is plotted *versus* time in Fig. 9B. The peak signal became progressively

smaller (and noisier) in each region presumably because of decreasing path length; however, it is clear that the dye signal was delayed in more distal regions. The fluorescence intensity was fitted with a sigmoidal curve (this was an empirical convenience to provide a smooth curve and has no mechanistic implication). The time at which this curve crosses +2 s.d. of the noise was used as an objective estimate of the first dye appearance in that region. These values are compared directly with the time course of the outward current in Fig. 9C. Thus for the D2 data point, the current measured at that time (~45 % of total) was accompanied by dye signal in the soma or dendritic regions proximal to D2. Conversely, the outward current had almost saturated (96 %) before any dye signal had appeared in region D3 or points beyond.

If the persistent outward current is generated by the same channels that are responsible for I_{sAHP}, there should be some correspondence between regions of the cell involved in these two events. To test this prediction we examined the spatial distribution of elevated $[Ca^{2+}]_i$ which triggers I_{sAHP}. Trains of action potentials were used in preference to voltage clamp commands to preserve the physiological pattern of soma/dendritic depolarization. The cell in Fig. 10A shows somatic and proximal apical dendritic regions of interest from which
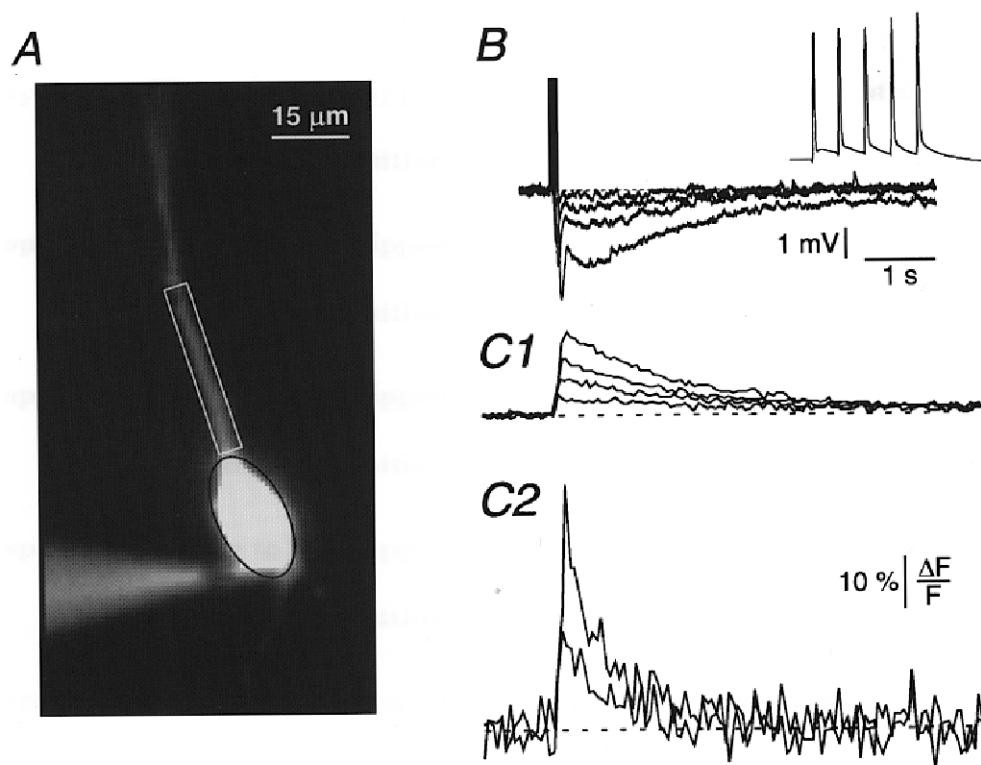

Figure 10. Location of $[Ca^{2+}]_i$ changes during slow afterhyperpolarizations
A, image of a fura-2-filled CA1 cell indicating regions of interest for single wavelength (380 nm) fluorescence measurements during action potential-evoked AHPs. B, current clamp recordings of the sAHP following 1, 3, 5 or 7 action potentials evoked by brief (2 ms) current injections at a frequency of 67 Hz (inset shows 5 spike train). C1, corresponding fluorescence measurements from the soma region on the same time scale as B. C2, dendritic region fluorescence measurements for the 3 and 7 spike trains. Scale bar applies to C1 and C2.

imaging data were obtained; these regions correspond to the areas largely responsible for chelator action determined previously (Fig. 9). The AHPs following 1, 3, 5 and 7 spikes are illustrated in Fig. 10B in comparison with the simultaneous fluorescence increases for the soma and dendrite (Fig. 10$C1$ and $C2$, respectively). The faster rate of recovery from $[Ca^{2+}]_i$ elevation in dendrites compared with the soma has been noted previously (Schiller *et al.* 1995). Extrapolation from ratiometric imaging in the same cell indicates that a 10% change in fluorescence is equal to a change in $[Ca^{2+}]_i$ of 51 nM. Thus action potential-evoked increases in $[Ca^{2+}]_i$ are detectable within the same regions that contribute to the chelator-induced outward current.

The bar graph in Fig. 11 provides a quantitative comparison of the properties of the persistent outward current. The histograms represent the peak outward current that was recorded under the various conditions. In addition to the complete block described for diazo-2 photolysis and β-adrenergic stimulation (Fig. 4) the persistent outward current was also sensitive to 8-Br cAMP and QX-314 in the pipette. As a comparison, the peak I_{sAHP} is also plotted. These data were obtained from the initial stages (before loss of the current) of recordings with diazo-2 or dibromo BAPTA and are, therefore, directly comparable data for the maximal I_{sAHP} that can be evoked by 80 ms depolarizing commands under these conditions (normal Ringer solution,

no blockers used). The conductance values associated with the outward currents were calculated after correction for individual voltage offsets in the recordings.

DISCUSSION

Identity of the outward current

The large conductance increase generated by BAPTA series calcium chelators has the properties of a tonically activated K$^+$ current with no clear voltage dependence between -50 and -100 mV. The current showed no requirement for depolarization and was observed to develop gradually during the first 5 min of whole-cell recording. In some cells there was a small decay of the current during a subsequent 10–30 min recording period. A number of persistent K$^+$ currents have been described in hippocampal neurones. Selyanko & Sim (1998) described a sustained K$^+$ current that was inhibited by raised Ca^{2+} and an increase in this current could explain our observations and be consistent with the observation that resting $[Ca^{2+}]_i$ decreases somewhat (75–25 nM, Fig. 8) during the initial stages of a recording, possibly due to buffering by fura-2. This mechanism is unlikely to contribute a significant component to our data because powerful Ca^{2+} buffering produces a smaller outward current than Ca^{2+} loading (Figs 7 and 11), which opposes the prediction for a Ca^{2+}-inhibited K$^+$ current.
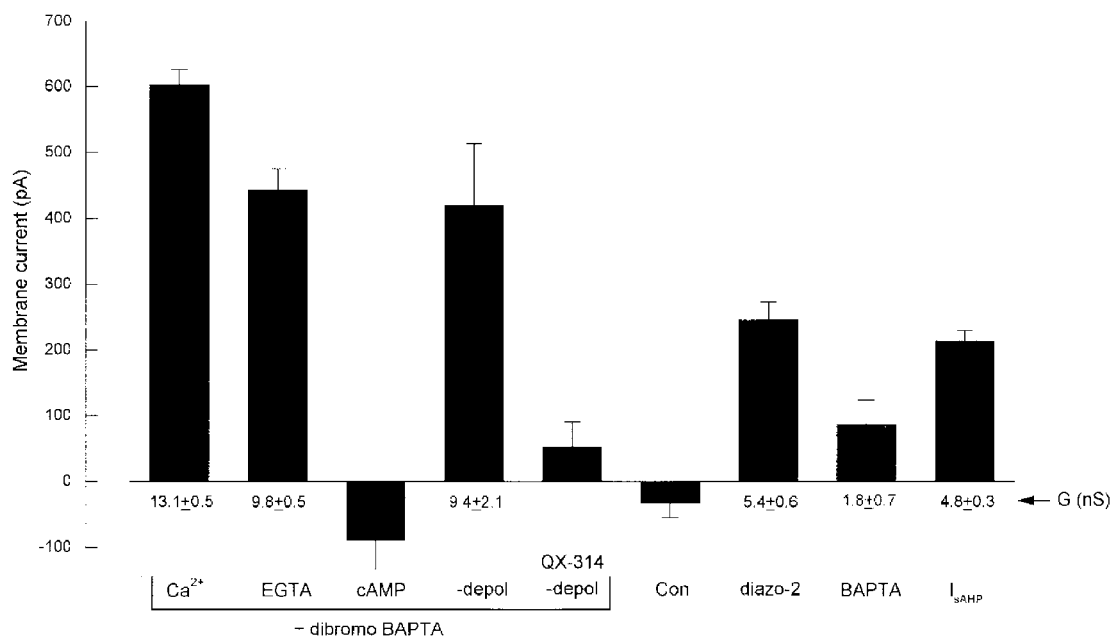

Figure 11. Action of BAPTA series chelators on holding current

The histogram plots maximal outward current recorded in the presence of BAPTA series chelators under various conditions compared with control data without buffer (con, $n = 10$) and the I_{sAHP} evoked by an 80 ms depolarization from -60 to -10 mV ($n = 21$). The dibromo BAPTA (1 mM) data set includes 50% Ca^{2+} loaded (Ca^{2+}, $n = 5$), with 10 mM EGTA (EGTA, $n = 5$), with 100 μM 8-Br cAMP (cAMP, $n = 7$), without depolarization ($-$depol) plus and minus 10 mM QX-314 ($n = 9$ and 5, respectively). Data for diazo-2 (2 mM, $n = 20$) and BAPTA itself (2 mM, $n = 6$) are also shown. The cAMP and QX-314 data are not significantly different from control data. Values of total conductance (G) were calculated after correcting for voltage offsets and are presented under the bars for the chelator data which are significantly different from control ($P < 0.01$).

A possible contribution from the persistent K$^+$ current I_M is ruled out because stimulation of β-noradrenergic receptors or the addition of a hydrolysis-resistant cAMP analogue blocked the outward current. The outward current as well as I_{sAHP} were blocked by intracellular QX-314. Although block of depolarization-evoked current could be due to the documented action of QX-314 on calcium current (Talbot & Sayer, 1996), the ability of this compound to abolish outward current in the absence of depolarization (Fig. 11) indicates a more direct action such as channel block. This would add to the promiscuity of this compound already known to affect many receptor and voltage-gated channels (Neher & Steinbach, 1978; Nathan *et al.* 1990; Oda *et al.* 1992; Perkins & Wong, 1995; Talbot & Sayer, 1996). The pharmacological profile of the outward current is the same as I_{sAHP} which is lost in tandem with outward current development. This loss of a depolarization-induced current could be ascribed to a shunting action of the conductance increase which depresses Ca^{2+} influx during depolarization. However, fura-2 fluorescence changes could still be observed in soma and dendrites after outward current development, which suggests that shunting was insufficient to prevent depolarization-evoked Ca^{2+} influx. It should also be noted that reductions in the AHP which result from reduced Ca^{2+} entry are not associated with changes in the time to peak of the current/potential, in contrast to the peak latency changes reported in this study and in previous publications (Lancaster & Zucker, 1994; Zhang *et al.* 1995). An alternative explanation to shunting is that I_{sAHP} was occluded by the outward current because it is the same conductance. This might arise if holding current changes are a consequence of greatly prolonged I_{sAHP} (Velumian & Carlen, 1999). Although chelator action was accompanied by an increased decay time of I_{sAHP}, this does not account for outward currents during voltage clamp at negative holding potentials without depolarization (Fig. 6). A persistently active slow AHP current is consistent with our observation that tonic outward current is generated in those parts of the cell (soma and dendrites) which appear to be responsible for the I_{sAHP} (Sah & Bekkers, 1996; this study, Figs 9 and 10). However, I_{sAHP} is demonstrably associated with elevated [Ca^{2+}]$_i$ (the exact mechanism is subject to debate, see Introduction) whereas a pharmacologically identical outward current appears not to require elevated [Ca^{2+}]$_i$ when induced by BAPTA series calcium chelators.

Actions of the chelators

The BAPTA series calcium chelators are capable of generating large outward currents in CA1 pyramidal cells. Diazo-2 and dibromo BAPTA (this study) as well as dimethyl BAPTA (Schwindt *et al.* 1992*b*; Zhang *et al.* 1995) are all capable of inducing this current as does BAPTA itself to a lesser degree (Velumian & Carlen, 1999; this study). While a reasonable first assumption is that the outward current is a consequence of the Ca^{2+} buffering characteristics of these compounds, any mechanism must account for the following data. Firstly, the outward current was not associated with elevated

[Ca^{2+}]$_i$, as demonstrated by the independence from depolarization, insensitivity to high EGTA and the lack of bulk [Ca^{2+}]$_i$ changes associated with activation or deactivation of the current. Secondly, the ability of the BAPTA series chelators to elicit outward currents showed no correlation with their K_D (Zhang *et al.* 1995; this study): dibromo and dimethyl BAPTA (K_D, 1·5 and 0·15 μM, respectively) produce large outward currents; diazo-2 (K_D, 2·2 μM) causes an intermediate outward current; whereas difluoro BAPTA and BAPTA (K_D, 1·7 and 0·21 μM, respectively) produce small or negligible outward current. Thus no clear relation exists between the Ca^{2+} buffering properties of these compounds and their ability to induce outward current.

Finally it is instructive to compare the actions of diazo-2 described here with those of diazo-4. In contrast to diazo-2, diazo-4 (unphotolysed K_D, 89 μM) does not hyperpolarize cells or result in loss of I_{sAHP} except after photolysis to the high affinity form (Lancaster & Zucker, 1994). In this case, block of I_{sAHP} was irreversible as expected following generation of a high affinity calcium chelator within the cell. Similarly, when the outward current produced by diazo-2 is deactivated by photolysis, the standard interpretation would be that this is a result of increased [Ca^{2+}]$_i$ buffering by the photolysis product. It is then difficult to explain the recovery of current in the presence of this high affinity buffer. Additionally, concurrent imaging revealed that photolysis-sensitive outward currents in excess of 400 pA are accompanied by only 6% decreases in calcium green-1 signals, whereas 100–200 pA I_{sAHP} accompany fluorescence changes of about 60% (data not shown but see also Lasser-Ross *et al.* 1997; Sah & Clements, 1999). Perhaps, therefore, the deactivation of outward current is a consequence not of [Ca^{2+}]$_i$ buffering but of the conformational change *per se*? A Ca^{2+}-insensitive action of diazo-2 photolysis on holding current may account for the apparent slow effects of diazo-2 photolysis on I_{sAHP} (Sah & Clements, 1999) which are observed in contrast to the rapid action of diazo-4, a compound lacking the additional variable of holding current changes (Lancaster & Zucker, 1994).

The initial development of outward current is similar to the time course of dye loading in these cells (Helmchen *et al.* 1996), but does this also explain the recovery time course following diazo-2 photolysis? The region of illumination includes a few millimetres of the recording pipette tip; therefore, the slow recovery of the outward current following photolysis is unlikely to be due to redistribution of unphotolysed chelator from the pipette. The recovery process might instead reflect a slow activation of outward current by the remaining, unphotolysed, diazo-2 within the cell.

This ensemble of observations is difficult to reconcile with Ca^{2+} buffering or [Ca^{2+}]$_i$ changes as the prime mechanism of chelator actions, although it is conceivable that we failed to resolve some highly localized or rapid [Ca^{2+}]$_i$ changes. The data also do not exclude some permissive role for the very

low resting $[Ca^{2+}]_i$ anticipated in the presence of EGTA. A facilitatory action of Ca^{2+} may then account for the difference between the action of low Ca^{2+} and Ca^{2+}-loaded chelator (Figs 7 and 11). Exogenous Ca^{2+} chelators are noted to prolong the time course of I_{sAHP} (peak latency and duration, Zhang *et al.* 1995). While no satisfactory explanation exists for this observation, it may be related to the underlying slow development of an outward current which receives a synergistic boost following Ca^{2+} influx (see Fig. 7). Speculation regarding a mechanism for chelator action might include the observation that BAPTA interacts with parvalbumin and calmodulin (Chiancone *et al.* 1986) and that there may be interactions among Ca^{2+}, the chelators and a Ca^{2+} binding site, so converting a normally transient process to a permanently active state. This might be achieved by a massive increase in Ca^{2+} sensitivity, as suggested to underlie the action of 1-ethyl-2-benzimidazolinone on inter-mediate conductance K_{Ca} channels expressed in cell lines (Pedersen *et al.* 1999).

Location of the outward current

The fura-2 fluorescence following onset of recording provides a picture of the areas of the cell which contribute to the outward current generated by co-diffusion of dibromo BAPTA from the electrode. The assumptions made for this interpretation are that fura-2 and dibromo BAPTA have similar mobility within the cell, and that there are no electro-physiological actions of dibromo BAPTA concentrations below the visible threshold of corresponding concentrations of fura-2. If these assumptions are valid then the outer limits for the outward current generation are no greater than 75 μm from the recording site. This represents an extreme limit since, as mentioned above, the time course of outward current development may be governed by the activation process rather than chelator distribution. The current plateau at this point may represent the maximal available conductance but it is possible that distal regions are electrically isolated due to a shunting action of the additional conductance which sets a detection limit on current generated in more distal regions.

Since the pharmacology of the outward current suggests some identity with I_{sAHP}, how does the location of I_{sAHP} compare with the persistent current? The location of I_{sAHP} is not well defined but some indication may be derived from the regions of $[Ca^{2+}]_i$ elevation associated with this event. When this is defined using natural spiking activity (this study; Knöpfel & Gähwiler, 1992; Lasser-Ross *et al.* 1997), the soma and proximal apical dendrites are the most likely location, which is consistent with electrophysiological data showing I_{sAHP} in apical dendrites (Andreasen & Lambert, 1995; Sah & Bekkers, 1996). Thus, the same areas of the cell are responsible for the chelator-induced outward current and I_{sAHP}. In this context it is worth noting that the ability of EGTA to inhibit I_{sAHP} generation within 1 min of recording (Fig. 7) suggests that the outward current contributing to

I_{sAHP} is generated by channels no greater than 50 μm from the site of recording (from Fig. 9C, assuming comparable diffusion of EGTA and fura-2), possibly including both somatic and immediately adjacent dendritic regions.

Functional implications for I_{sAHP}

The pharmacology of the outward current is indicative of a tonically active sAHP current, although we do not exclude the formal possibility that it may be comprised in whole, or part, of a previously unidentified and separate current with the same pharmacological characteristics as I_{sAHP}. The inhibition of this outward current via β-noradrenergic receptors and cAMP occurs in the absence of Ca^{2+} elevation or influx. The transduction mechanism, therefore, acts on targets which are downstream of voltage-dependent Ca^{2+} entry, possibly at the K^+ channel itself in addition to noradrenergic actions on L-type Ca^{2+} channel reopening (Cloues *et al.* 1997; Marrion & Tavalin, 1998). Assuming that a persistently active I_{sAHP} is responsible for the observations reported here, the activity of this current can be dissociated from $[Ca^{2+}]_i$ changes. This raises the question of whether the persistent activation by chelators is recruiting part of the physiological mechanism of channel activation.

Ca^{2+} release following flash photolysis suggests rapid activation (Lancaster & Zucker, 1994), but recent experiments in the presence of apamin indicate that the rapid activation phase is followed by a slow component (Sah & Clements, 1999, their Fig. 4b) which was modelled by slow gating of the channel. A more complex regulation of this current has also been suggested to result from indirect, downstream, actions of Ca^{2+} (Schwindt *et al.* 1992a). Although there is some similarity of I_{sAHP} to the time course of mean dendritic $[Ca^{2+}]_i$ during spike trains (Helmchen *et al.* 1996), discrepancy between the time course of fluorescence signals and the current following depolarization has been noted (Lasser-Ross *et al.* 1997), which is exacerbated by the presence of BAPTA (Jahromi *et al.* 1999). Clearly, the early stages of volume-averaged Ca^{2+} signals are unlikely to report accurately the Ca^{2+} concentration changes in sub-membrane shells adjacent to membrane channels (Llinás *et al.* 1992; Monck *et al.* 1994; Eilers *et al.* 1995). This could account for early discrepancies in time course but is unlikely to be relevant during later stages of the response. Thus precedents exist for divorcing $[Ca^{2+}]_i$ from I_{sAHP} and the persistent current may be an interesting manifestation of a physiological mechanism but we have no direct evidence to support this possibility.

The much larger conductance seen with Ca^{2+}-loaded dibromo BAPTA compared with I_{sAHP} might be taken as evidence for a different current. Although these experiments were executed without K^+ channel blockers and are comparable to I_{sAHP} recorded following brief spike trains (Lancaster & Adams, 1986), supranormal I_{sAHP} can be evoked in the presence of tetraethylammonium which causes spike broadening by blocking BK channels so Ca^{2+} influx is much

greater than observed under normal conditions. This suggests that physiologically relevant spiking activity utilises a fraction of the available sAHP conductance, and the data with Ca^{2+}-loaded dibromo BAPTA provide an estimate of the total conductance that is available in these cells (Fig. 11). The operational fraction of sAHP conductance is similar to the estimates obtained from noise analysis in dentate granule cells (Valiante *et al.* 1997). This apparently under-utilised conductance may be activated by synaptically mediated Ca^{2+} influx or during conditions such as anoxic hyperpolarization which is associated with Ca^{2+}-activated K^+ current (Yamamoto *et al.* 1997; Erdemli *et al.* 1998).

The location of outward current $< 100 \ \mu m$ from the somatic recording is interposed between most dendritic excitatory input and the axonal output. Accumulation of $[Ca^{2+}]_i$ is prominent in this area following high frequency spiking (Helmchen *et al.* 1996) and would be expected to activate I_{sAHP}. The increased membrane conductance following short spike bursts will be anticipated to downgrade the influence of subsequent synaptic input from the whole apical dendritic tree. Conversely, transmitter inhibition of I_{sAHP} is likely to enhance transfer of electrical signals between the soma and dendrites of pyramidal cells.

ADAMS, S. R., KAO, J. P. Y. & TSIEN, R. Y. (1989). Biologically useful chelators that take up Ca^{2+} upon illumination. *Journal of the American Chemical Society* **111**, 7957–7968.

ANDREASEN, M. & LAMBERT, J. D. C. (1995). The excitability of CA1 pyramidal cell dendrites is modulated by a local Ca^{2+}-dependent K^+ conductance. *Brain Research* **698**, 193–203.

BARRETT, J. N., MAGLEBY, K. L. & PALLOTTA, B. (1982). Properties of single calcium activated potassium channels in cultured rat muscle. *Journal of Physiology* **331**, 211–230.

CHIANCONE, E., THULIN, E., BOFFI, A., FORSEN, S. & BRUNORI, M. (1986). Evidence for the interaction between the calcium indicator 1,2-bis(*o*-aminophenoxy)ethane-N,N,N′,N′-tetraacetic acid and calcium-binding proteins. *Journal of Biological Chemistry* **261**, 16306–16308.

CLOUES, R. K., TAVALIN, S. J. & MARRION, N. V. (1997). *β*-Adrenergic stimulation selectively inhibits long-lasting L-type calcium channel facilitation in hippocampal pyramidal neurons. *Journal of Neuroscience* **17**, 6493–6503.

EILERS, J., CALLEWAERT, G., ARMSTRONG, C. & KONNERTH, A. (1995). Calcium signalling in a narrow somatic submembrane shell during synaptic activity in cerebellar Purkinje neurons. *Proceedings of the National Academy of Sciences of the USA* **92**, 10272–10276.

ERDEMLI, G., XU, Y. Z. & KRNJEVIC, K. (1998). Potassium conductance causing hyperpolarization of CA1 hippocampal neurons during hypoxia. *Journal of Neurophysiology* **80**, 2378–2390.

GRYNKIEWICZ, G., POENIE, M. & TSIEN, R. Y. (1985). A new generation of Ca^{2+} indicators with greatly improved fluorescence properties. *Journal of Biological Chemistry* **260**, 3440–3450.

HELMCHEN, F., IMOTO, K. & SAKMANN, B. (1996). Ca^{2+} buffering and action potential-evoked Ca^{2+} signalling in dendrites of pyramidal neurons. *Biophysical Journal* **70**, 1069–1081.

JAHROMI, B. S., ZHANG, L., CARLEN, P. L. & PENNEFATHER, P. (1999). Differential time course of slow afterhyperpolarizations and associated Ca^{2+} transients in rat CA1 pyramidal neurons: further dissociation by Ca^{2+} buffer. *Neuroscience* **88**, 719–726.

KNÖPFEL, T. & GÄHWILER, B. H. (1992). Activity-induced elevations of intracellular calcium concentration in pyramidal and nonpyramidal cells of the CA3 region of rat hippocampal slice cultures. *Journal of Neurophysiology* **68**, 961–963.

KÖHLER, M., HIRSCHBERG, B., BOND, C. T., KINZIE, J. M., MARRION, N. V., MAYLIE, J. & ADELMAN, J. P. (1996). Small-conductance calcium-activated potassium channels from mammalian brain. *Science* **273**, 1709–1714.

LANCASTER, B. & ADAMS, P. R. (1986). Calcium-dependent current generating the afterhyperpolarization of hippocampal neurons. *Journal of Neurophysiology* **55**, 1268–1282.

LANCASTER, B. & BATCHELOR, A. M. (1999). Action of BAPTA-derived Ca^{2+} buffers on intrinsic membrane currents in CA1 neurones. *Society for Neuroscience Abstracts* **25**, 192.

LANCASTER, B. & ZUCKER, R. S. (1994). Photolytic manipulation of Ca^{2+} and the time course of slow Ca^{2+}-activated K^+ current in rat hippocampal neurons. *Journal of Physiology* **475**, 229–239.

LASSER-ROSS, N., ROSS, W. N. & YAROM, Y. (1997). Activity-dependent $[Ca^{2+}]_i$ changes in guinea-pig vagal motoneurons: relationship to the slow afterhyperpolarization. *Journal of Neurophysiology* **78**, 825–834.

LLINÁS, R., SUGIMORI, M. & SILVER, B. (1992). Microdomains of high calcium concentration in a presynaptic terminal. *Science* **256**, 677–679.

MADISON, D. V. & NICOLL, R. A. (1986). Cyclic adenosine 3′,5′-monophosphate mediates *β*-receptor actions of noradrenaline in rat hippocampal pyramidal cells. *Journal of Physiology* **372**, 245–259.

MARRION, N. V. & TAVALIN, S. J. (1998). Selective activation of Ca^{2+}-activated K^+ channels by co-localized Ca^{2+} channels in hippocampal neurons. *Nature* **395**, 900–905.

MONCK, J. R., ROBINSON, I. M., ESCOBAR, A. L., VERGARA, J. L. & FERNANDEZ, J. M. (1994). Pulsed laser imaging of rapid Ca^{2+} gradients in excitable cells. *Biophysical Journal* **67**, 505–514.

MULKEY, R. M. & ZUCKER, R. S. (1993). Calcium released by photolysis of DM-nitrophen triggers transmitter release at the crayfish neuromuscular junction. *Journal of Physiology* **462**, 243–260.

NATHAN, T., JENSEN, M. S. & LAMBERT, J. D. C. (1990). The slow inhibitory postsynaptic potential in rat hippocampal CA1 neurones is blocked by intracelluar injection of QX-314. *Neuroscience Letters* **110**, 309–313.

NEHER, E. & STEINBACH, J. H. (1978). Local anaesthetics transiently block currents through single acetylcholine receptor channels. *Journal of Physiology* **277**, 153–176.

ODA, M., YOSHIDA, A. & IKEMOTO, Y. (1992). Blockade by local anaesthetics of the single Ca^{2+}-activated K^+ channel in rat hippocampal neurones. *British Journal of Pharmacology* **105**, 63–70.

PEDARZANI, P. & STORM, J. F. (1993). PKA mediates the effects of monoamine transmitters on the K^+ current underlying the slow spike frequency adaptation in hippocampal neurons. *Neuron* **11**, 1023–1035.

PEDERSEN, K. A., SCHRØDER, R. L., SKAANING-JENSEN, B., STRØBAEK, D., OLESEN, S.-P. & CHRISTOPHERSEN, P. (1999). Activation of the human intermediate-conductance Ca^{2+}-activated K^+ channel by 1-ethyl-2-benzimidazolinone is strongly Ca^{2+}-dependent. *Biochimica et Biophysica Acta* **1420**, 231–240.

PERKINS, K. L. & WONG, R. K. S. (1995). Intracellular QX-314 blocks the hyperpolarization-activated inward current I_q in hippocampal CA1 pyramidal cells. *Journal of Neurophysiology* **73**, 911–915.

PETHIG, R., KUHN, M., PAYNE, R., ADLER, E., CHEN, T. H. & JAFFE, L. F. (1989). On the dissociation constants of BAPTA-type calcium buffers. *Cell Calcium* **10**, 491–498.

SAH, P. & BEKKERS, J. M. (1996). Apical dendritic location of slow afterhyperpolarization current in hippocampal pyramidal neurons: implications for the integration of long-term potentiation. *Journal of Neuroscience* **16**, 4537–4542.

SAH, P. & CLEMENTS, J. D. (1999). Photolytic manipulation of $[Ca^{2+}]_i$ reveals slow kinetics of potassium channels underlying the afterhyperpolarization in hippocampal pyramidal neurons. *Journal of Neuroscience* **19**, 3657–3664.

SAH, P. & McLACHLAN, E. M. (1991). Ca^{2+}-activated K^+ currents underlying the afterhyperpolarization in guinea pig vagal neurons: a role for Ca^{2+}-activated Ca^{2+} release. *Neuron* **7**, 257–264.

SCHILLER, J., HELMCHEN, F. & SAKMANN, B. (1995). Spatial profile of dendritic calcium transients evoked by action potentials in rat neocortical pyramidal neurones. *Journal of Physiology* **487**, 583–600.

SCHWINDT, P. C., SPAIN, W. J. & CRILL, W. E. (1992*a*). Calcium-dependent potassium currents in neurons from cat sensorimotor cortex. *Journal of Neurophysiology* **67**, 216–226.

SCHWINDT, P. C., SPAIN, W. J. & CRILL, W. E. (1992*b*). Effects of intracellular calcium chelation on voltage-dependent and calcium-dependent currents in cat neocortical neurons. *Neuroscience* **47**, 571–578.

SELYANKO, A. A. & SIM, J. A. (1998). Ca^{2+}-inhibited non-inactivating K^+ channels in cultured rat hippocampal pyramidal neurones. *Journal of Physiology* **510**, 71–91.

STOCKER, M., KRAUSE, M. & PEDARZANI, P. (1999). An apamin-sensitive Ca^{2+}-activated K^+ current in hippocampal pyramidal neurons. *Proceedings of the National Academy of Sciences of the USA* **96**, 4662–4667.

TALBOT, M. J. & SAYER, R. J. (1996). Intracellular QX-314 inhibits calcium currents in hippocampal CA1 pyramidal neurons. *Journal of Neurophysiology* **76**, 2120–2124.

TANABE, M., GÄHWILER, B. H. & GERBER, U. (1998). L-type Ca^{2+} channels mediate the slow Ca^{2+}-dependent afterhyperpolarization current in rat CA3 pyramidal cells *in vitro. Journal of Neurophysiology* **80**, 2268–2273.

VALIANTE, T. A., ABDUL-GHANI, M. A., CARLEN, P. L. & PENNEFATHER, P. (1997). Analysis of current fluctuations during after-hyperpolarization current in dentate granule neurones of the rat hippocampus. *Journal of Physiology* **499**, 121–134.

VELUMIAN, A. A. & CARLEN, P. L. (1999). Differential control of three after-hyperpolarizations in rat hippocampal neurones by intracellular calcium buffering. *Journal of Physiology* **517**, 210–216.

XIA, X.-M., FAKLER, B., RIVARD, A., WAYMAN, G., JOHNSON-PAIS, T., KEEN, J. E., ISHII, T., HIRSCHBERG, B., BOND, C. T., LUTSENKO, S., MAYLIE, J. & ADELMAN, J. P. (1998). Mechanism of calcium-gating in small-conductance calcium-activated potasium channels. *Nature* **395**, 503–507.

YAMAMOTO, S., TANAKA, E. & HIGASHI, H. (1997). Mediation by intracellular calcium-dependent signals of hypoxic hyperpolarization in rat hippocampal CA1 neurons *in vitro. Journal of Neurophysiology* **77**, 386–392.

YOSHIDA, A., ODA, M. & IKEMOTO, Y. (1991). Kinetics of the Ca^{2+}-activated K^+ channels in rat hippocampal neurons. *Japanese Journal of Physiology* **41**, 297–315.

ZHANG, L., PENNEFATHER, P., VELUMIAN, A., TYMIANSKI, M., CHARLTON, M. & CARLEN, P. L. (1995). Potentiation of a slow Ca^{2+}-dependent K^+ current by intracellular Ca^{2+} chelators in hippocampal CA1 neurons of rat brain slices. *Journal of Neurophysiology* **74**, 2225–2241.

ZHANG, L., WEINER, J. L., VALIANTE, T. A., VELUMIAN, A., WALSON, P., JAHROMI, S. S., SCHETZER, S., PENNEFATHER, P. & CARLEN, P. L. (1994). Whole-cell recording of the Ca^{2+}-dependent slow afterhyperpolarization in hippocampal neurones: effects of internally applied anions. *Pflügers Archiv* **426**, 247–253.

Corresponding author

B. Lancaster: Wolfson Institute for Biomedical Research, Cruciform Building, University College London, Gower Street, London WC1E 6BT, UK.

Email: b.lancaster@ucl.ac.uk

Author's present address

A. M. Batchelor: Department of Physiology, University College London, Gower Street, London WC1E 6BT, UK.